E. SOAVE,[1] V. CORRE,[1,2] C. RAVENSBERGEN,[1,3] J.H. HAN,[1,4] M. KREYER,[1] E. KIRILOV,[1,5] R. GRIMM[1,5]

[1] Institute of Experimental Physics, University of Innsbruck
(Technikerstraße 25, 6020 Innsbruck, Austria; e-mail: elisa.soave@uibk.ac.at)
[2] Present address: Safran Reosc
(Sain-Pierre-du-Perray 91280, France)
[3] Present address: ColdQuanta, Oxford Centre for Innovation
(OX1 1BY, United Kingdom)
[4] Present address: Korea Research Institute of Standards and Science
(Daejeon 34113, South Korea)
[5] Institute for Quantum Optics and Quantum Information (IQOQI), Austrian Academy of Sciences
(Technikerstraße 21a, 6020 Innsbruck, Austria)

LOW-FIELD FESHBACH RESONANCES AND THREE-BODY LOSSES IN A FERMIONIC QUANTUM GAS OF ^{161}Dy

UDC 539

We report on the high-resolution Feshbach spectroscopy on a degenerate, spin-polarized Fermi gas of ^{161}Dy atoms, measuring three-body recombination losses at a low magnetic field. For field strengths up to 1 G, we identify as much as 44 resonance features and observe the plateaus of very low losses. For four selected typical resonances, we study the dependence of the three-body recombination rate coefficient on the magnetic resonance detuning and on the temperature. We observe a strong suppression of losses with decreasing temperature already for small detunings from the resonance. The characterization of complex behavior of the three-body losses of fermionic ^{161}Dy is important for future applications of this peculiar species in research on atomic quantum gases.

Keywords: ultracold Fermi gases, Feshbach resonances, three-body recombination.

1. Introduction

Over the past decade, the exotic interactions of submerged-shell lanthanide atoms have tremendously boosted experimental research on ultracold quantum gases [1]. Exciting properties of such atoms result from long-range anisotropic interactions in combination with the tunability of the contact interaction via magnetically controlled Feshbach resonances [2]. Prominent examples for novel states of matter created in the laboratory are quantum ferrofluids of Dy [3] and supersolids realized with both Dy and Er [4–6]. Progress has also been made with quantum-gas mixtures of different lanthanide atoms (Dy–Er) [7, 8] and mixtures of lanthanide and alkali-metal atoms (Dy–K) [9, 10], with a wide potential for future experiments on exotic states of quantum matter.

For interaction control, magnetic lanthanide atoms offer a rich spectrum of Feshbach resonances [11–14], much denser as compared to alkali-metal atoms. This experimentally well-established fact is a consequence of the anisotropy stemming both from the strong magnetic dipole-dipole interaction and from the van-der-Waals interaction for electronic ground

states with non-zero orbital angular momentum [15, 16]. The anisotropic interaction leads to a strong mixing of different partial waves. If a hyperfine structure is present, such as for the fermionic isotopes ^{161}Dy and ^{167}Er, the Feshbach spectrum is even more complex, and the blessing of tunability may turn into a curse of omnipresent three-body recombination losses.

The experiments performed with ^{161}Dy in our laboratory are motivated by the prospect to realize novel superfluid states in mass-imbalanced fermion mixtures [17–19]. In a Fermi–Fermi mixture of ^{161}Dy and ^{40}K atoms, we have recently demonstrated hydrodynamic behavior as a manifestation of strong interactions, realized on top of an interspecies Feshbach resonance [10]. Further experiments are in progress on the formation of bosonic Feshbach molecules, paired fermionic many-body states, and collective behavior of the strongly interacting mixture. In all these experiments, the Dy–Dy intraspecies Feshbach resonances represent a complication, and appropriate strategies have to be developed to minimize unwanted effects such as three-body losses and heating.

Feshbach resonances in spin-polarized fermionic quantum gases result from the scattering in odd partial waves. Accordingly, p-wave resonances have been observed in early experimental work [20–22] and studied theoretically [23, 24]. More recent experiments [25, 26] have provided deeper insights into the scaling laws and universal properties of three-body recombination losses near p-wave resonances. Our present situation of ^{161}Dy, however, is more complex because of the strong coupling between different partial waves and a possible interaction between different closely spaced or overlapping resonances, which makes a theoretical description very challenging. Experiments are needed to find out to what extent our resonances in ^{161}Dy behave in a similar way.

In this article, we report on the experimental investigation of the ultradense Feshbach spectrum of ^{161}Dy at low magnetic field strength (up to about 1 G) with high resolution ($\sim$1 mG). To minimize the effect of finite collision energies, i.e., broadening effects and the influence of higher partial waves, we work in the deeply quantum-degenerate regime at rather low values of the Fermi energy down to a few 100 nK. In Sect. 2, we present the Feshbach loss spectrum, exhibiting nearly 50 loss features in a 1-G-wide interval. We also identify plateaus of very low losses, which can be used for efficient evaporative cooling. In Sect. 3, we then present the results of studies of four typical resonances, where we report on the dependence of the three-body rate coefficient on the magnetic detuning and the temperature of the sample. Our measurements show that even very small detunings from the resonance of a few mG are sufficient to enter a regime where losses are strongly suppressed with decreasing temperature.

2. Low-field Feshbach Spectrum

2.1. Sample preparation

All our experiments begin with the production of a degenerate Fermi gas of ^{161}Dy atoms. We follow the procedures described in detail in Ref. [9]: After capturing the atoms in a magneto-optical trap (MOT) operated at the 626-nm intercombination line [27], the sample is transferred into a crossed-beam optical dipole trap (ODT), which uses near-infrared light at a wavelength of 1064 nm. Here, forced evaporative cooling is performed by ramping down the trapping potential. Under optimized conditions, we obtain a sample of up to $N = 1.5 \times 10^5$ atoms in a nearly harmonic trap (geometrically averaged trap frequency $\bar{\omega} = 2\pi \times 150$ Hz) at a temperature $T = 80$ nK. With the Fermi temperature $T_{\mathrm{F}} = \hbar\bar{\omega}(6N)^{1/3}/k_{\mathrm{B}} = 695$ nK, this corresponds to deeply degenerate conditions with $T/T_{\mathrm{F}} = 0.12$ and the peak number density $\hat{n} = 1.6 \times 10^{14}/\mathrm{cm}^3$ in the center of the trap. Our sets of measurements are taken over typically many hours (sometimes even a few days), where long-term drifts may reduce the maximum atom number provided by roughly a factor of two. In a last preparation stage, the ODT is modified by replacing one of the laser beams (horizontally propagating) with a beam of larger waist. This modification provides us with more flexibility to vary the trap frequency $\bar{\omega}$ and, in particular, it allows us to realize very shallow traps to work at lower atomic number densities. For each experiment, the trap is chosen in a way to avoid residual evaporation. The particular conditions for each set of measurements are listed in App. A.

The cloud is fully spin-polarized in the lowest hyperfine Zeeman sub-level $|F, m_{\mathrm{F}}\rangle = |21/2, -21/2\rangle$ as a result of optical pumping during the MOT stage [28] and the subsequent rapid dipolar relaxation of a residual population in higher spin states in the ODT [29]. For the fully spin-polarized sample, inelastic two-body losses are suppressed already at very

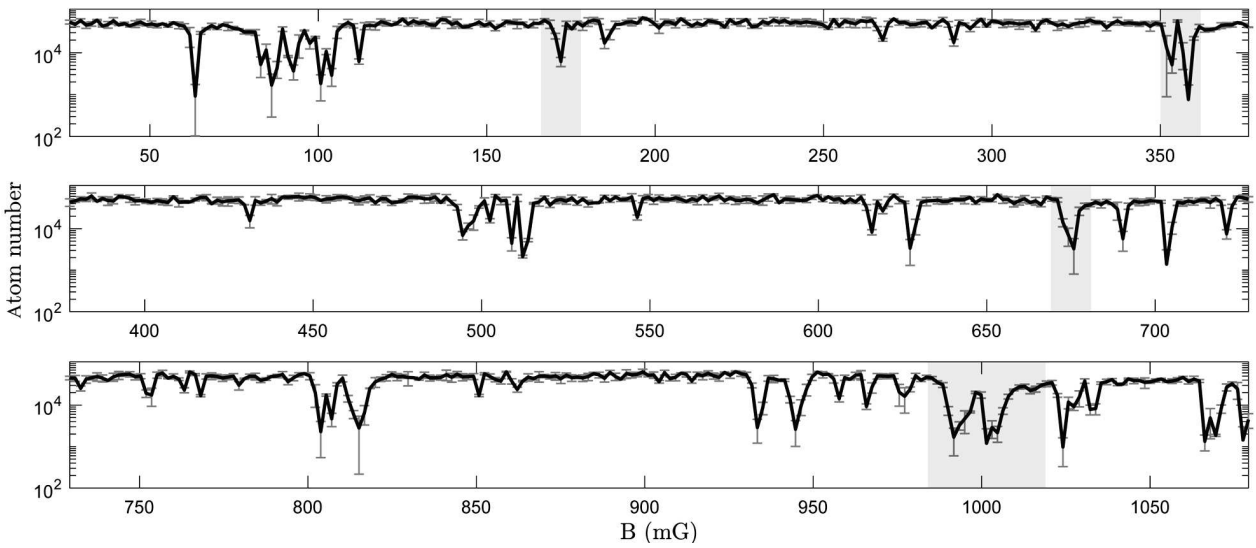

Fig. 1. Low-field Feshbach spectrum of a degenerate sample of spin-polarized ^{161}Dy. The magnetic field is varied in steps of 1.6 mG. The error bars show the sample standard deviation of three individual measurements at the same magnetic field. We observe about 44 loss features, which we attribute to Feshbach resonances. The shaded areas correspond to the four resonances that are investigated in detail in Sect. 3

low magnetic field values. The minimization of three-body losses, essential for efficient evaporative cooling, depends very sensitively on the particular magnetic field applied. Our evaporation sequence is performed at a magnetic bias field of 230 mG, which we found to work slightly better than at 430 mG, as applied in Ref. [9].

2.2. Loss scan

We study the low-field Feshbach spectrum by measuring atom losses for a variable magnetic field strength [2] in the interval between 0 and 1 G. After the preparation of the sample in a very shallow ODT (for experimental parameters see App. A), we ramp the magnetic field from the evaporation field to the variable target one in 20 ms. The low trap frequency of $\bar{\omega} = 2\pi \times 100$ Hz is chosen to minimize losses induced by the magnetic field ramp. We hold the cloud for 7 s, and then release it from the ODT. An absorption image is taken after a time of flight of 10 ms.

The magnetic-field stability is essential for resolving narrow loss features. Using radio-frequency spectroscopy [1] we identified a 50-Hz ripple in the ambient magnetic field as the main source of noise, with a peak-to-peak value of 1.7 mG. Other noise sources, such as the noise in the current of our coils, stay well below an estimated rms level of 1 mG.

In Fig. 1 we plot the remaining atom number as a function of the magnetic field. We count $\simeq$44 loss features, which we assign to Feshbach resonances. On resonance, the three-body recombination rate is greatly enhanced and leads to the reduction in the atom number by a factor of more than 10. At these positions, we also observe substantial heating (not shown). The resonances seem to mostly gather in groups, with flat, typically tens of mG wide, plateaus between them. Within these plateaus, losses are rather weak and stay within a few percent even for the long hold time of 7 s applied.

The recorded Feshbach spectrum resembles previous observations in submerged-shell lanthanide atoms (Er [11, 14], Dy [12, 13], Tm [30]), which are known to exhibit a dense and very complex resonance spectrum. In the cases of the fermionic isotopes ^{161}Dy and ^{167}Er, where a hyperfine structure is present, the resonance density is extremely high. While for ^{167}Er, a density of about 25 resonances per gauss has been reported in the interval between 0 and 4.5 G [11], previous work on ^{161}Dy has revealed between about 10 resonances per gauss in the interval between 0 and

[1] We investigate the magnetic-field stability by performing radio-frequency spectroscopy on ^{40}K. The possibility to work with potassium in the same setup follows from the fact that our apparatus is designed for mixture experiments [9, 10].

6 G [12] and up to about 100 resonances in a 250-mG wide interval near 34 G [13]. With our 44 resonances in the interval between 0 and 1 G, we apparently resolve more resonances than in Ref. [12], which we attribute to our higher magnetic field resolution. We believe that a further improved magnetic field stability to well below 2 mG would reveal even more resonances and a substructure of some of our observed features. The complex spectrum of resonances may be further analyzed using statistical methods [14, 30], which is beyond the scope of the present work.

3. Case Studies of Selected Resonances

We now perform a systematic investigation of the K_3 coefficient as a function of the magnetic-field and the temperature for selected resonances. In Sect. 3.1, we first show how, from atom number decay measurements, we obtain the value of the three-body recombination coefficient K_3. In Sections 3.2 and 3.3, we investigate the dependence of K_3 on the magnetic field and the initial temperature, respectively.

3.1. Three-body decay curves and loss-rate coefficients

In the absence of two-body losses, the evolution of the number of trapped atoms $N(t)$ can be modeled based on the differential equation

$$\dot{N}(t) = -\Gamma_v N(t) - 3K_3 \int d^3r\, n^3(\mathbf{r}, t), \qquad (1)$$

where Γ_v is the one-body loss rate from collisions with rest-gas particles, and $n(\mathbf{r}, t)$ represents the number density distribution of the cloud. The quantity K_3 denotes the three-body event rate coefficient, which, for a single atomic species, is related to the commonly used three-body loss rate coefficient by $L_3 = 3K_3$. Note that, according to our phenomenological definition, the K_3 coefficient represents a thermal average over the distribution of collision energies in the sample, and does not represent the coefficient for a specific collision energy as used in theoretical work [31]. For our experiments, we estimate a rest-gas limited lifetime as long as $1/\Gamma_v \simeq 60$ s. Given such a low one-body loss rate, Γ_v can be neglected in the analysis of near-resonance decay curves, while it is relevant for cases on the long-lived plateaus.

In Fig. 2 we show three typical decay curves, on resonance (a), near a resonance (b) and far away from any resonance (c). The sample is held in the ODT at a fixed magnetic field. After a variable hold time, the cloud is released, and the number of remaining atoms is measured by time-of-flight imaging. To analyze the decay curves and to extract values for K_3, we apply a heuristic model (for details, see App. B) to

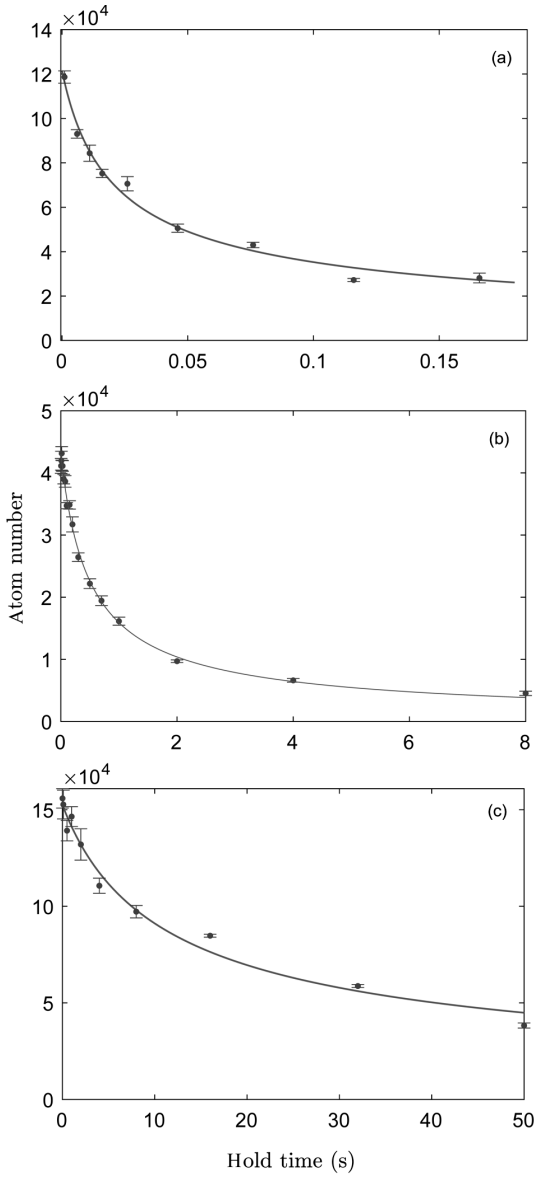

Fig. 2. Typical decay curves. The measurements have been performed on resonance at $B = 678$ mG (a), for small detuning at $B = 989$ mG (b), and on a minimum-loss plateau at $B = 225$ mG (c). The solid lines show fits by the heuristic model introduced in App. B

quantify the initial slope $\dot{N}(0)$. From the initial decay rate $1/\tau = -\dot{N}(0)/N(0)$ and knowledge of the experimental parameters at $t = 0$, we then calculate the resulting values for K_3. This approach, which focuses on the initial decay, avoids complications by the heating of the sample during the decay. Depending on the experimental conditions under consideration, decay times can vary from a few ms to many seconds. As an example, the measurement reported in Fig. 2, *a* was carried out under typical experimental conditions (see App. A) very close to the center of the 679-mG resonance, with initially about 1.2×10^5 atoms. Our fit yields an initial decay time $\tau = 22(6)$ ms, and, for the three-body rate coefficient, we obtain $K_3 = 4(1) \times 10^{-26}$ cm^6/s. The same measurement, performed few mG detuned from the resonance at 995 mG and reported in Fig. 2, *b*, already shows a significantly longer decay time ($\tau = 0.50(9)$ s). We calculate a three-body recombination coefficient value $K_3 = 7(2) \times^{-28}$ cm^6/s, two orders of magnitude lower than on resonance.

The measurement in Fig. 2, *c* is carried out at a magnetic field of 225 mG, on a minimum-loss plateau, and reveals a very long lifetime. To observe the effect of three-body losses, we worked in a tightly compressed trap with $\bar{\omega} = 2\pi \times 380$ Hz, leading to a peak-density of $\hat{n}_0 \approx 6 \times 10^{14}$/cm^3, which is exceptionally high for a degenerate Fermi gas. We measure an initial decay time $\tau = 12(3)$ s, from which a value $K_3 = 5(3) \times 10^{-32}$ cm^6/s is obtained. This value is extraordinary low, which is highlighted by comparison with ^{87}Rb as a widely used bosonic species, where the K_3 coefficient has been measured to be of the order of 10^{-29} cm^6/s [32, 33]. Such an extremely weak three-body decay, together with the sizeable elastic scattering cross-section from dipolar collisions [34], explains why Fermi gases of submerged-shell lanthanide atoms facilitate highly efficient evaporative cooling [9, 35].

3.2. Dependence on magnetic-field detuning

In this Section, we discuss selected loss features as typical examples for the many resonances observed in our Feshbach spectrum. We focus on three resonant features that lead to relatively strong losses in the measured Feshbach spectrum (near 358 mG, 677 mG, and 999 mG, see loss scan in Fig. 1). For reference, we also investigate a weaker loss resonance (near 170 mG), which appears to be well isolated from other resonances. We consider their line shapes and widths by presenting measurements on the K_3 values as a function of the magnetic detuning from resonance. Here, we work in the deeply degenerate regime, with $T/T_F \simeq 0.2$ at a low $T_F \simeq 400$ nK (for details, see App. A), which minimizes line broadening stemming from the finite kinetic energy [14, 36]. Our results are displayed in Fig. 3, *a–d*. The measured values for K_3 vary over more than four orders of magnitude. Maximum values are found to exceed 10^{-25} cm^6/s. The presence of weak one-body losses (see Sect. 3.1) imposes a lower limit for the measurable K_3 value, which, for this particular trapping conditions, is in the range of a few 10^{-30} cm^6/s. This lower limit is indicated by the dashed horizontal lines in Fig. 3.

Figure 3, *a* shows the resonance near 170 mG, which is the weakest of the four selected features. We observe a full width of about 3.5 mG [2]. The line shape is essentially symmetric, which may first appear surprising in view of the expected asymmetric line shapes of Feshbach resonances in higher partial waves, which usually show a sharp edge on the lower side (marking the resonance position) along with a tail on the upper side [36–39]. We assume that the shape of the weak feature is dominated by the magnetic-field fluctuations in our experimental setup (see Sect. 2.2), which may affect the observed loss features in an interval of a few mG. The fluctuations will smear out any narrower feature and mask the true resonance line shape (see the discussion on broadening effects in App. C). This interpretation is supported by the fact that we never observe any narrower feature. Therefore, we believe that the observed behavior of narrower resonances, such as the 170-mG feature, is dominated by magnetic-field fluctuations.

In Fig. 3, *b*, we show a double feature of two resonances, separated by about 4 mG. While the weaker feature near 355 mG closely resembles the one in Fig. 2, *a*, the stronger feature near 359 mG shows a peak value for K_3 exceeding 10^{-25} cm^6/s, which is an order of magnitude higher. The stronger feature also shows indications of the tail expected on the upper side for such resonances. The resonance appears to be

[2] We define the width as the full magnetic field range where the K_3 value exceeds the geometric average between its maximum and minimum. This corresponds to the full width at half maximum on a logarithmic scale.

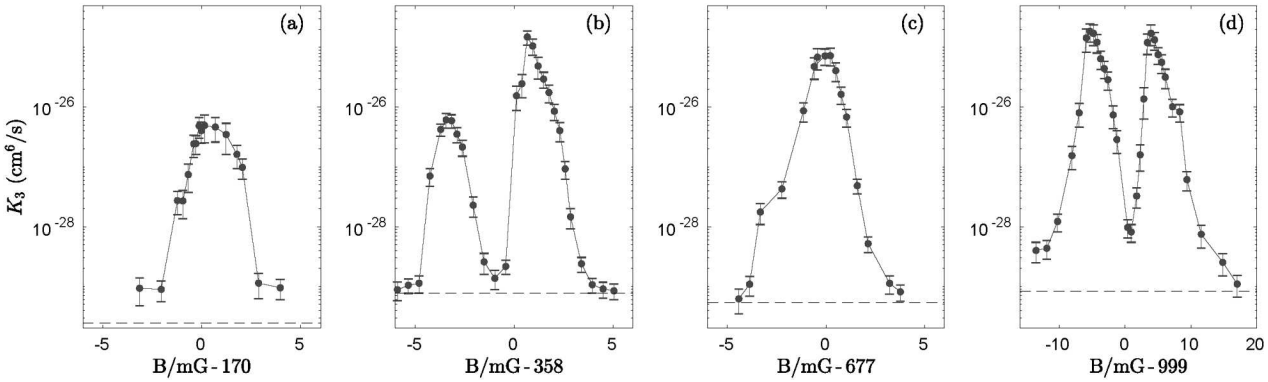

Fig. 3. K_3 coefficient as a function of the magnetic-field, measured for the four selected resonances. Note that in (*a–c*) the full range covers 12 mG, whereas in (*d*) it is three times wider. Each data point is obtained from an individual decay curve as discussed in Sect. 3.1. The dashed lines indicate the lower limit to the measurable K_3 value, imposed by one-body losses

wide enough that its true structure is not fully masked by the magnetic-field fluctuations. Figure 3, *c* shows a feature near 677 mG, which in the Feshbach scan in Fig. 1, appeared to be a single, relatively strong resonance. A closer investigation, however, reveals a shoulder on the lower side, which is likely to be caused by another weak overlapping resonance. On the upper side, the K_3 coefficient falls off in a way resembling the expected tail. Figure 3, *d* finally displays our strongest observed loss feature; note the three times wider magnetic-field interval. We see a double feature separated by about 10 mG. The line shapes of the two resonances correspond to the expectation of a sharper edge on the lower side and a tail on the upper side. Here, at least for these broader features, magnetic-field fluctuations do not have a substantial effect on the line shape.

3.3. Temperature dependence

We now turn our attention to the dependence of the K_3 coefficient on the temperature of the cloud, for different magnetic detunings from the resonance center. We vary the temperature of the cloud by interrupting the evaporation sequence in a controlled way and by adiabatically varying the final trap frequency. For these measurements, decay is observed in a 160-Hz and a 400-Hz trap, for lower and higher temperatures, respectively. The K_3 coefficient is obtained according to Eq. (B3) or Eq. (B2), depending on the initial T/T_F of the sample. We introduce the effective temperature $\tilde{T}$, such that the mean energy per particle is $3k_\mathrm{B}\tilde{T}$. This definition takes into account that, for a degenerate Fermi gas, the relative momentum and, thus, the collision energy stay finite even at $T = 0$. In the limit of a thermal gas, $\tilde{T} = T$ holds, while, for a degenerate one, we have $\tilde{T} = T\,\mathrm{Li}_4(-\zeta)/\mathrm{Li}_3(-\zeta)$ [40], where ζ is the fugacity, and Li_i is the polylogarithm of order i.

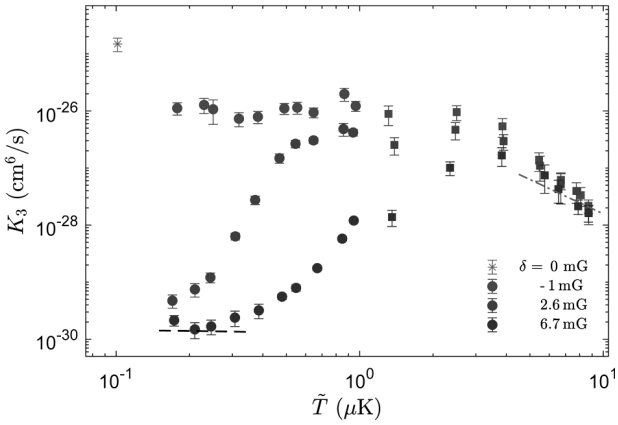

Fig. 4. Temperature dependence of K_3, for various detunings (typical uncertainty 0.2 mG) relative to the center of the 358-mG resonance. For $\tilde{T} \lesssim 1$ μK the samples have initial $T/T_\mathrm{F} < < 1$. The decay curves have been measured in a $\bar{\omega}/2\pi = 160$-Hz (circles) and 400-Hz trap (squares). As a reference, we plot the K_3 resonant peak value, corresponding to the maximum in Fig. 3, *b*. The dot-dashed line shown for $T > 5$ μK indicates the T^{-2} dependence, according to Eq. (2), with $\zeta = 0.022$. The dashed line indicates the lower limit to the measurable K_3 value, imposed by one-body losses

Figure 4 indicates the behavior of the K_3 value as a function of $\tilde{T}$ for three different magnetic detunings relative to the center of the 358-mG resonance.

We first discuss the K_3 behavior in the high-energy regime ($\tilde{T} \gtrsim 3$ μK). Here, the three curves decrease in a similar manner, showing no dependence on the magnetic field. Such a behavior reflects the unitarity limit for the K_3 coefficient, which was predicted and observed in several resonantly interacting systems, fermionic and bosonic ones (e.g., [25, 41–44]). A non-degenerate atomic system enters the unitarity-limited regime when the thermal de Broglie wavelength $\lambda_{\mathrm{dB}} = \hbar\sqrt{2\pi/(mk_{\mathrm{B}}T)}$ becomes comparable to a characteristic length associated with the resonance at a given magnetic detuning [3]. We attribute to the competition between those two length scales the fact that the larger the detuning, the higher is the temperature at which the K_3 value enters the unitary regime. In this regime, the K_3 value is expected to scale as T^{-2} [23]:

$$K_3 = \zeta \frac{12\sqrt{3}\pi^2\hbar^5}{m^3(k_{\mathrm{B}}T)^2}. \qquad (2)$$

The prefactor ζ relates to the efficiency of three colliding atoms forming a dimer and a free atom, and is believed to be a non-universal (i.e., species-dependent) quantity. A fit to our data, considering only the points with $\tilde{T} > 5$ μK, yields a value $\zeta = 0.022(2)$. In Ref. [26], the authors extracted a value $\zeta = 0.09$ for ^{6}Li. Those two results are about an order of magnitude below what has been observed for Bose gases, where values of $\zeta = 0.9$, 0.3, and 0.24 have been derived for ^{7}Li [41], ^{39}K [42], and ^{164}Dy [43], respectively.

We now discuss the temperature-dependence of K_3 far below the unitarity-limited regime. Figure 4 demonstrates that even a very small magnetic resonance detuning of a few mG can have a dramatic effect on the low-temperature behavior. The data taken at $\delta = 6.7$ mG (typical uncertainty 0.2 mG) show a reduction of K_3 from a maximum value of the order of 10^{-27} cm^6/s at $\tilde{T} = 3.5\,\mu$K to a minimum of about 10^{-30} cm^6/s at $\tilde{T} \lesssim 200$ nK. Note that the minimum value that we can observe is limited by one-body decay (dashed line), so that the true suppression will be even larger. A very similar behavior is observed closer to the resonance at $\delta = 2.6$ mG. Here, a maximum K_3 value of $\sim 5 \times 10^{-27}$ cm^6/s is found at $\tilde{T}$ of the order of 1 μK, which is reduced by three orders of magnitude at our lowest temperature $\tilde{T} \approx 200$ nK. The main effect of the smaller detuning appears to be a shift of the qualitatively similar behavior to lower temperatures.

These observations on the low-temperature behavior can be compared with recent experimental work studying the three-body recombination on p-wave Feshbach resonances in ^{6}Li [25, 26]. For the limit of very low collision energies E_{coll}, a threshold law $K_3 \propto \propto E_{\mathrm{coll}}^2$, as originally predicted in Ref. [23], has been observed in Ref. [25] for a thermal ($T/T_{\mathrm{F}} > 1$) Fermi gas, where $K_3 \propto T^2$. This observation of threshold-law behavior required a relatively large resonance detuning. In our case, with rather small detunings, the threshold-law regime would require extremely low collision energies. This regime, however, remains inaccessible in our present experiments because of two limitations: The Fermi energy gives a lower limit to the collision energy ($\tilde{T} = T_{\mathrm{F}}/4$ at $T = 0$), and one-body losses do not allow us to measure K_3 values below $\sim 10^{-30}$ cm^6/s. However, beyond the threshold-law regime, we observe the same steep increase with temperature as seen in Ref. [25] for relatively large magnetic detunings. The breakdown of the threshold law has been interpreted [25] in terms of the effective range of the resonance.

The case very close to the resonance (data points for $\delta = -1$ mG in Fig. 4) reveals a different behavior. Here, we do not observe any loss suppression with decreasing temperature. The K_3 value appears to level off at about 10^{-26} cm^6/s. This, however, does not rule out the possibility of the loss suppression at values of $\tilde{T}$ that are even lower than what we can realize experimentally in the deeply degenerate situation. The single data point shown for $\delta = 0$ at $\tilde{T} \approx 75$ nK corresponds to the loss maximum in Fig. 3, *b*. This measurement highlights that three-body losses can be very strong on the top of a resonance, suggesting no suppression at low temperatures. A similar on-resonance behavior has been observed in Refs. [21, 26], but, in contrast to our work, these experiments were limited to the non-degenerate case.

In the narrow detuning range of $|\delta| \lesssim 1$ mG, the interpretation of our present results is impeded by the sensitivity of the experiments to magnetic field noise

[3] The length scale that characterizes the interaction is the scattering length a for an s-wave resonance and by $\sqrt{|V_p|k_{\mathrm{eff}}}$ in the case of p-wave Feshbach resonances. Here, V_p and k_{eff} are the scattering volume and the effective range, respectively.

Experimental parameters for the different sets of measurements: geometrically averaged trap frequency $\bar{\omega}$, atom number N, temperature T, Fermi temperature T_F, reduced temperature T/T_F, the function $\beta(x)$ according to Eq. (B4), and the peak density $\hat{n}$. All quantities represent the initial values after preparation (at $t = 0$)

Figure	$\bar{\omega}/2\pi$, Hz	N	T, nK	T_F, nK	T/T_F	$\beta(T/T_F)$	$\hat{n}$, cm^{-3}
Fig. 1	100	5×10^4	70	320	0.21	0.616	4.8×10^{13}
Fig. 2, *a*	58	$1.22(4) \times 10^5$	29(3)	250	0.12	0.84	3.1×10^{13}
Fig. 2, *b*	120	$4.3(1) \times 10^4$	83(3)	367	0.23	0.59	5.7×10^{13}
Fig. 2, *c*	380	$1.53(3) \times 10^5$	358(8)	1.77×10^3	0.20	0.63	6×10^{14}
Fig. 3, *a*	88	$\simeq 1.2 \times 10^5$	64	379	0.17	0.72	6×10^{13}
Fig. 3, *b*	118	$\simeq 4 \times 10^4$	77	352	0.22	0.59	5×10^{13}
Fig. 3, *c*	118	$4 - 6 \times 10^4$	77–88	352–403	0.22	0.59	$5 - 6 \times 10^{13}$
Fig. 3, *d*	118	$\simeq 5 \times 10^4$	106	379	0.28	0.46	5.2×10^{13}
Fig. 5, *a*, stars	118	$\simeq 4 \times 10^4$	77	352	0.22	0.59	5×10^{13}
Fig. 5, *a, b*, diamonds	157	$4.5 - 6 \times 10^4$	86–126	487–536	0.16–0.26	0.50–0.74	$0.78 - 1 \times 10^{14}$
Fig. 5, *b*, squares	157	$4 - 5.5 \times 10^4$	88–187	468–520	0.17–0.4	0.26–0.71	$0.6 - 1 \times 10^{14}$

(see Sect. 2.2 and App. C). The on-resonance behavior of the three-body recombination at ultralow collision energies, which has also been subject to recent theoretical investigations [45], thus remains a topic for the future research.

4. Conclusions

In summary, we have carried out Feshbach spectroscopy on an optically trapped spin-polarized degenerate Fermi gas of ^{161}Dy atoms by measuring three-body recombination losses. We have focused on the interval of low magnetic fields up to 1 G, scanned with a high resolution on the order of 1 mG. The ultradense loss spectrum revealed a stunning complexity with 44 resolved loss features, some of them showing up in groups and other ones appearing as isolated individual features. We also observed low-loss plateaus, which are typically a few 10 mG wide and which are free of resonances. Here, very low three-body losses facilitate the highly efficient evaporative cooling.

We have studied selected resonance features in more details by measuring the three-body recombination rate coefficient K_3 upon a variation of the magnetic resonance detuning and the temperature. In general, the observed behavior shows strong similarities with recent observations on p-wave Feshbach resonances [25,26]. At higher temperatures (above a few μK), we observed the unitarity limitation of resonant three-body losses. At low temperatures in the nanokelvin range, we observed a strong suppression of losses with decreasing temperature, provided a small detuning of just a few mG is applied. Right on the top of the resonance, however, three-body losses remain very strong even at the lowest temperatures we can realize.

Our work shows that, in experiments employing fermionic ^{161}Dy gases, a special attention must be payed to choosing and controlling the magnetic field in a way to avoid detrimental effects of three-body recombination losses. For our specific applications targeting at strongly interacting fermion mixtures of ^{161}Dy and ^{40}K [10], those magnetic-field regions are of particular interest, where one can combine near-resonant interspecies Dy–K interaction with low-loss regions of Dy.

We acknowledge support by the Austrian Science Fund (FWF) within Projects No. P32153-N36 and P34104-N, and within the Doktoratskolleg ALM (W1259-N27). We further acknowledge a Marie Sklodowska Curie fellowship awarded to J.H.H. by the European Union (project SIMIS, Grant Agreement No. 894429). We thank the members of the ultracold atom groups in Innsbruck for many stimulating discussions and for sharing technological know how.

APPENDIX A.
Summary of the initial experimental conditions

In the Table, we report the experimental conditions under which the measurements reported in Figs. 1, 2, 3 and 5 have been carried out. For the measurement in Fig. 4, where the

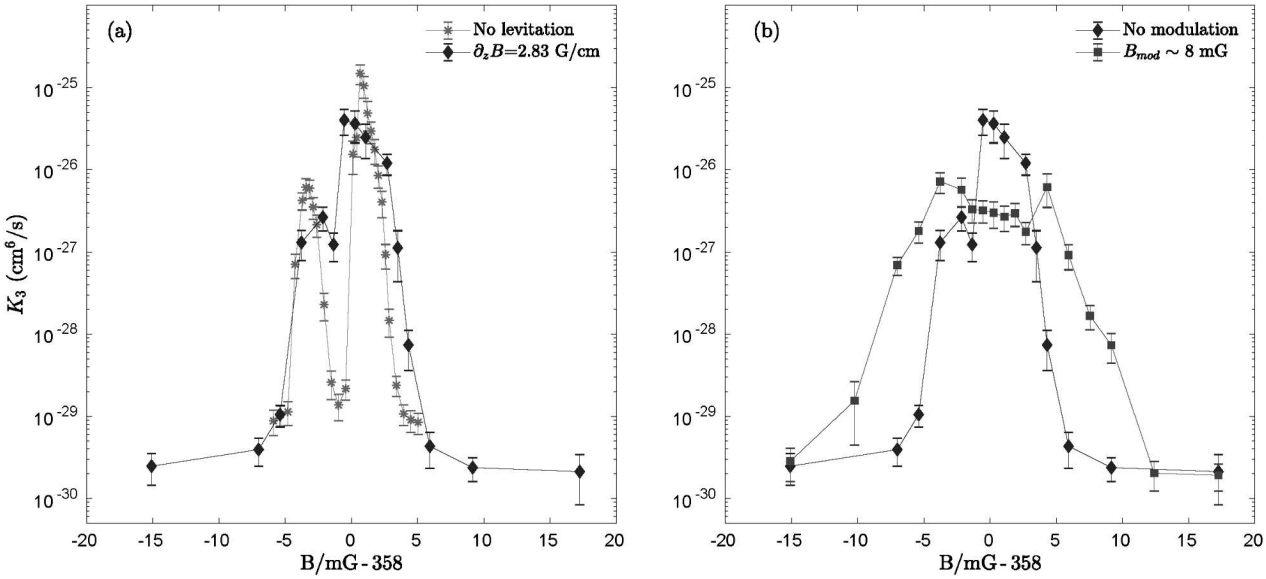

Fig. 5. Effect of magnetic field broadening. The K_3 value is plotted versus the magnetic field, in the region around 358 mG. Effect of the magnetic field gradient used for levitating Dy (*a*). Effect of a sinusoidal magnetic field modulation, with a frequency of 600 Hz and an peak-to-peak amplitude of 8 mG (*b*)

value of K_3 as a function of the $\tilde{T}$ is reported, the different temperatures have been achieved by interrupting the evaporation in a controlled way. This unavoidably has led to initial experimental conditions which vary over a wide range. The initial atom number ranges from 5×10^4 to 10^6. The coldest samples have $T/T_{\rm F} \simeq 0.18$ and peak densities $\hat{n} \simeq 10^{14}$ cm^{-3}.

APPENDIX B.
Extraction of the loss-rate coefficient

Here we summarize our method to extract values for the three-body rate coefficient K_3 from the decay curves. Basically the same procedures have been applied in Ref. [10].

The particles that are more likely to collide and leave the trap are the ones in the center of the trap, with highest density and lowest potential energy. Therefore losses are accompanied by heating of the cloud, which is known as antievaporation heating in the thermal case [46] or hole heating in the case of a degenerate Fermi gas [47]. As a consequence the shape of the density distribution $n(\mathbf{r}, t)$ changes with time. Taking a time-dependent temperature $T(t)$ into account, Eq. (1) leads to a set of coupled differential equations (see for instance [46]). We circumvent this complication by focusing on the initial decay rate $1/\tau = -\dot{N}(0)/N(0)$, where $N(0) = N_0$ and $\dot{N}(0)$ represent the atomic number and its time derivative, respectively, both at $t = 0$. For the initial decay and thus the decay time τ only the initial number density distribution $n_0(\mathbf{r}) = n(\mathbf{r}, t = 0)$ is relevant.

Neglecting one-body losses and considering only the initial part of the decay, Eq. (1) leads to

$$K_3 = \frac{N(0)}{3\tau} \left(\int d^3r \, n_0^3(\mathbf{r}) \right)^{-1}. \tag{B1}$$

For the limit of a thermal (Gaussian) distribution [46], the integration results in

$$K_3 = \sqrt{3} \frac{T_0^3}{\tau N_0^2} \left(\frac{2\pi k_{\rm B}}{m\bar{\omega}^2} \right)^3. \tag{B2}$$

Here $\hbar$ is the reduced Planck constant, $k_{\rm B}$ is the Boltzmann constant, m is the atomic mass, and T_0 is the initial temperature of the sample. For the number density distribution of a degenerate Fermi gas, we find

$$K_3 = \frac{3\pi^4}{4} \frac{1}{\tau N_0} \left(\frac{\hbar}{m\bar{\omega}} \right)^3 \frac{1}{\beta(T_0/T_{\rm F})}. \tag{B3}$$

The function $\beta(T/T_{\rm F})$ is defined as the three-body integral of a finite-temperature Fermi gas normalized to the zero-temperature case:

$$\beta(T/T_{\rm F}) = \frac{\int d^3\mathbf{r} \, n^3(\mathbf{r})}{\int d^3\mathbf{r} \, n_{\rm TF}^3(\mathbf{r})}, \tag{B4}$$

where $n(\mathbf{r})$ describes the density profiles of non-interacting fermion systems at finite temperature, and $n_{\rm TF}(\mathbf{r})$ refers to the Thomas–Fermi profile at $T = 0$. By numerical integration, we find that the function can be well approximated numerically for $x = T/T_{\rm F} \lesssim 1$ by $\beta(x) \simeq (1 + 12.75x^2 + 31.05x^4 - 8.46x^6)^{-1}$.

In order to obtain the initial decay rate, we fit the decay curve with

$$N(t) = \frac{N_0}{\sqrt[\alpha-1]{1 + (\alpha - 1)t/\tau}}, \tag{B5}$$

which is the solution of the differential equation $\dot{N}/N_0 = -\tau^{-1} (N/N_0)^\alpha$ for decay by few-body process of order α.

This heuristic model allows us to access the initial time decay τ without making an assumption on the true order of the loss process. The fit parameter α absorbs the order n of the recombination process together with effects from heating. The initial atom number N_0 is also derived from the fit, whereas the initial temperature T_0 is measured separately. The value of K_3 is finally obtained from Eq. (B2) or Eq. (B3).

APPENDIX C. Broadening effects

When dealing with a dense Feshbach spectrum of narrow resonances, it is important to understand and possibly eliminate potential broadening effects. In our system, we identify two sources of broadening: magnetic levitation and magnetic field noise. In experiments where a decrease of the trapping frequencies leads to a trapping potential not deep enough to hold atoms against gravity, magnetic field levitation is often used to cancel (or reduce) the gravitational sag [48]. However, the presence of a magnetic field gradient introduces an inhomogeneity of the magnetic field along the vertical extent of the cloud. Assuming full levitation for dysprosium ($\partial_z B = 2.83$ G/cm) and a typical Thomas–Fermi radius $\sim$10 μm, our atomic sample is subjected to a magnetic-field variation of $\sim$6 mG over the trap volume. In Fig. 5, *a*, we demonstrate the effect of levitation broadening on the K_3 coefficient. We work at the 358-mG resonance. If no gradient is applied, we can resolve a double-peak structure. The two features have a full width of about 2 mG, with peak values of $6(3) \times 10^{-27}$ and $1.5(4) \times 10^{-25}$ cm^6/s, respectively. The presence of the magnetic field gradient reduces the resolution and the two peaks almost merge into a single feature 7.7-mG wide. We can still distinguish two local maxima, whose values are reduced with respect to the no-levitation case. In view of this broadening effect, we decided to carry out all measurements reported in the main text without magnetic levitation. To achieve low enough trap frequencies in the shallow trap where the atoms are transferred at the end of the evaporation, we employ the second ODT stage with an increased waist of the horizontal trapping beam, as mentioned in Sect. 2.1. Such a trap geometry allows us to reach low trapping frequencies without too much sacrificing the trap depth.

In another set of measurements, we investigate the effect of magnetic field fluctuations. We artificially introduce noise into the system by adding a sinusoidal magnetic field modulation to the bias field. We chose a modulation frequency of 600 Hz, i.e. faster than the trap frequencies, but still slow enough to avoid technical complications. We then measure decay curves for different modulation strengths and magnetic field detunings. In Fig. 5, *b* we report the obtained K_3 values versus magnetic field detunings for 10-mG peak to peak modulation. As a reference, we plot the K_3 profile measured in the absence of artificial noise. The modulation results in a broadening of the feature and consequent loss of field resolution. The peak value decreases and the curve flattens off.

Regardless of the source of broadening, a magnetic-field inhomogeneity (in time and space) has an averaging effect on the K_3 coefficient, and leads to a broadening and weakening of the narrow loss features characterizing the dysprosium Feshbach spectrum.

1. L. Chomaz, I. Ferrier-Barbut, F. Ferlaino, B. Laburthe-Tolra, B.L. Lev, T. Pfau. Dipolar physics: A review of experiments with magnetic quantum gases. Preprint arXiv:2201.02672 (2022).
2. C. Chin, R. Grimm, P. Julienne, E. Tiesinga. Feshbach resonances in ultracold gases. *Rev. Mod. Phys.* **82**, 1225 (2010).
3. H. Kadau, M. Schmitt, M. Wenzel, C. Wink, T. Maier, I. Ferrier-Barbut, T. Pfau. Observing the Rosensweig instability of a quantum ferrofluid. *Nature* **530**, 194 (2016).
4. L. Tanzi, E. Lucioni, F. Fam'a, J. Catani, A. Fioretti, C. Gabbanini, R.N. Bisset, L. Santos, G. Modugno. Observation of a dipolar quantum gas with metastable supersolid properties. *Phys. Rev. Lett.* **122**, 130405 (2019).
5. F. Böttcher, J.-N. Schmidt, M. Wenzel, J. Hertkorn, M. Guo, T. Langen, T. Pfau. Transient supersolid properties in an array of dipolar quantum droplets. *Phys. Rev. X* **9**, 011051 (2019).
6. L. Chomaz, D. Petter, P. Ilzhöfer, G. Natale, A. Trautmann, C. Politi, G. Durastante, R.M.W. van Bijnen, A. Patscheider, M. Sohmen, *et al.* Long-lived and transient supersolid behaviors in dipolar quantum gases. *Phys. Rev. X* **9**, 021012 (2019).
7. A. Trautmann, P. Ilzhöfer, G. Durastante, C. Politi, M. Sohmen, M.J. Mark, F. Ferlaino. Dipolar quantum mixtures of erbium and dysprosium atoms. *Phys. Rev. Lett.* **121**, 213601 (2018).
8. C. Politi, A. Trautmann, P. Ilzhöfer, G. Durastante, M.J. Mark, M. Modugno, F. Ferlaino. Interspecies interactions in an ultracold dipolar mixture. *Phys. Rev. A* **105**, 023304 (2022).
9. C. Ravensbergen, V. Corre, E. Soave, M. Kreyer, E. Kirilov, R. Grimm. Production of a degenerate Fermi-Fermi mixture of dysprosium and potassium atoms. *Phys. Rev. A* **98**, 063624 (2018).
10. C. Ravensbergen, E. Soave, V. Corre, M. Kreyer, B. Huang, E. Kirilov, R. Grimm. Resonantly interacting Fermi-Fermi mixture of ^{161}Dy and 40 K. *Phys. Rev. Lett.* **124**, 203402 (2020).
11. A. Frisch, M. Mark, K. Aikawa, F. Ferlaino, J.L. Bohn, C. Makrides, A. Petrov, S. Kotochigova. Quantum chaos in ultracold collisions of gas-phase erbium atoms. *Nature* **507**, 475 (2014).
12. K. Baumann, N.Q. Burdick, M. Lu, B.L. Lev. Observation of low-field Fano-Feshbach resonances in ultracold gases of dysprosium. *Phys. Rev. A* **89**, 020701(R) (2014).
13. N.Q. Burdick, Y. Tang, B.L. Lev. Long-lived spin-orbit-coupled degenerate dipolar Fermi gas. *Phys. Rev. X* **6**, 031022 (2016).
14. T. Maier, H. Kadau, M. Schmitt, M. Wenzel, I. Ferrier-Barbut, T. Pfau, A. Frisch, S. Baier, K. Aikawa, L. Chomaz,

et al. Emergence of chaotic scattering in ultracold Er and Dy. *Phys. Rev. X* **5**, 041029 (2015).
15. A. Petrov, E. Tiesinga, S. Kotochigova. Anisotropy induced Feshbach resonances in a quantum dipolar gas of highly magnetic atoms. *Phys. Rev. Lett.* **109**, 103002 (2012).
16. S. Kotochigova. Controlling interactions between highly magnetic atoms with Feshbach resonances. *Rep. Prog. Phys.* **77**, 093901 (2014).
17. K. Gubbels, H. Stoof. Imbalanced Fermi gases at unitarity. *Phys. Rep.* **525**, 255 (2013).
18. J. Wang, Y. Che, L. Zhang, Q. Chen. Enhancement effect of mass imbalance on Fulde–Ferrell–Larkin–Ovchinnikov type of pairing in Fermi-Fermi mixtures of ultracold quantum gases. *Sci. Rep.* **7**, 39783 (2017).
19. M. Pini, P. Pieri, R. Grimm, G.C. Strinati. Beyond-mean-field description of a trapped unitary Fermi gas with mass and population imbalance. *Phys. Rev. A* **103**, 023314 (2021).
20. C.A. Regal, C. Ticknor, J.L. Bohn, D.S. Jin. Tuning p-wave interactions in an ultracold Fermi gas of atoms. *Phys. Rev. Lett.* **90**, 053201 (2003).
21. J. Zhang, E.G.M. van Kempen, T. Bourdel, L. Khaykovich, J. Cubizolles, F. Chevy, M. Teichmann, L. Tarruell, S.J.J.M.F. Kokkelmans, C. Salomon. P-wave Feshbach resonances of ultracold ^{6}Li. *Phys. Rev. A* **70**, 030702 (2004).
22. C. H. Schunck, M.W. Zwierlein, C.A. Stan, S.M.F. Raupach, W. Ketterle, A. Simoni, E. Tiesinga, C.J. Williams, P.S. Julienne. Feshbach resonances in fermionic ^{6}Li. *Phys. Rev. A* **71**, 045601 (2005).
23. H. Suno, B.D. Esry, C.H. Greene. Recombination of three ultracold fermionic atoms. *Phys. Rev. Lett.* **90**, 053202 (2003).
24. F. Chevy, E.G.M. van Kempen, T. Bourdel, J. Zhang, L. Khaykovich, M. Teichmann, L. Tarruell, S.J.J.M.F. Kokkelmans, C. Salomon. Resonant scattering properties close to a p-wave Feshbach resonance. *Phys. Rev. A* **71**, 062710 (2005).
25. J. Yoshida, T. Saito, M. Waseem, K. Hattori, T. Mukaiyama. Scaling law for three-body collisions of identical fermions with p-wave interactions. *Phys. Rev. Lett.* **120**, 133401 (2018).
26. M. Waseem, J. Yoshida, T. Saito, T. Mukaiyama. Unitarity-limited behavior of three-body collisions in a p-wave interacting Fermi gas. *Phys. Rev. A* **98**, 020702 (2018).
27. T. Maier, H. Kadau, M. Schmitt, A. Griesmaier, T. Pfau. Narrow-line magneto-optical trap for dysprosium atoms. *Opt. Lett.* **39**, 3138 (2014).
28. D. Dreon, L. Sidorenkov, C. Bouazza, W. Maineult, J. Dalibard, S. Nascimbene. Optical cooling and trapping highly magnetic atoms: The benefits of a spontaneous spin polarization. *J. Phys. B* **50**, 065005 (2017).
29. M. Lu, N.Q. Burdick, B.L. Lev. Quantum degenerate dipolar Fermi gas. *Phys. Rev. Lett.* **108**, 215301 (2012).
30. V.A. Khlebnikov, D.A. Pershin, V.V. Tsyganok, E.T. Davletov, I.S. Cojocaru, E.S. Fedorova, A.A. Buchachenko, A.V. Akimov. Random to chaotic statistic transformation in low-field Fano–Feshbach resonances of cold thulium atoms. *Phys. Rev. Lett.* **123**, 213402 (2019).
31. B.D. Esry, C.H. Greene, H. Suno. Threshold laws for three-body recombination. *Phys. Rev. A* **65**, 010705 (2001).
32. E.A. Burt, R.W. Ghrist, C.J. Myatt, M.J. Holland, E.A. Cornell, C.E. Wieman. Coherence, correlations, and collisions: What one learns about Bose–Einstein condensates from their decay. *Phys. Rev. Lett.* **79**, 337 (1997).
33. J. Söding, D. Gu'ery-Odelin, P. Desbiolles, F. Chevy, H. Inamori, J. Dalibard. Three-body decay of a rubidium Bose–Einstein condensate. *Appl. Phys. B* **69** (1999).
34. J.L. Bohn, M. Cavagnero, C. Ticknor. Quasi-universal dipolar scattering in cold and ultracold gases. *New J. Phys.* **11**, 055039 (2009).
35. K. Aikawa, A. Frisch, M. Mark, S. Baier, R. Grimm, F. Ferlaino. Reaching Fermi degeneracy via universal dipolar scattering. *Phys. Rev. Lett.* **112**, 010404 (2014).
36. A. Green, H. Li, J.H. See Toh, X. Tang, K.C. McCormick, M. Li, E. Tiesinga, S. Kotochigova, S. Gupta. Feshbach resonances in p-wave three-body recombination within Fermi-Fermi mixtures of open-shell ^{6}Li and closed-shell ^{173}Yb atoms. *Phys. Rev. X* **10**, 031037 (2020).
37. C. Ticknor, C.A. Regal, D.S. Jin, J.L. Bohn. Multiplet structure of Feshbach resonances in nonzero partial waves. *Phys. Rev. A* **69**, 042712 (2004).
38. T. Nakasuji, J. Yoshida, T. Mukaiyama. Experimental determination of p-wave scattering parameters in ultracold ^{6}Li atoms. *Phys. Rev. A* **88**, 012710 (2013).
39. J. Li, J. Liu, L. Luo, B. Gao. Three-body recombination near a narrow Feshbach resonance in ^{6}Li. *Phys. Rev. Lett.* **120**, 193402 (2018)
40. 40. B. DeMarco. *Quantum Behavior of an Atomic Fermi Gas. Ph.D. thesis* (University of Colorado, 2001).
41. B.S. Rem, A.T. Grier, I. Ferrier-Barbut, U. Eismann, T. Langen, N. Navon, L. Khaykovich, F. Werner, D.S. Petrov, F. Chevy, *et al.* Lifetime of the Bose gas with resonant interactions. *Phys. Rev. Lett.* **110**, 163202 (2013).
42. R.J. Fletcher, A.L. Gaunt, N. Navon, R.P. Smith, Z. Hadzibabic. Stability of a unitary Bose gas. *Phys. Rev. Lett.* **111**, 125303 (2013).
43. T. Maier, I. Ferrier-Barbut, H. Kadau, M. Schmitt, M. Wenzel, C. Wink, T. Pfau, K. Jachymski, P.S. Julienne. Broad universal Feshbach resonances in the chaotic spectrum of dysprosium atoms. *Phys. Rev. A* **92**, 060702 (2015).
44. U. Eismann, L. Khaykovich, S. Laurent, I. Ferrier-Barbut, B.S. Rem, A.T. Grier, M. Delehaye, F. Chevy, C. Salomon, L.-C. Ha. Universal loss dynamics in a unitary Bose gas. *Phys. Rev. X* **6**, 021025 (2016).
45. M. Schmidt, H.-W. Hammer, L. Platter. Three-body losses of a polarized Fermi gas near a p-wave Feshbach resonance in effective field theory. *Phys. Rev. A* **101**, 062702 (2020).
46. T. Weber, J. Herbig, M. Mark, H.-C. Nägerl, R. Grimm. Three-body recombination at large scattering lengths in an ultracold atomic gas. *Phys. Rev. Lett.* **91**, 123201 (2003).
47. E. Timmermans. Degenerate fermion gas heating by hole creation. *Phys. Rev. Lett.* **87**, 240403 (2001).

48. T. Weber, J. Herbig, M. Mark, H.-C. Nägerl, R. Grimm. Bose–Einstein condensation of cesium. *Science* **299**, 232 (2003).

Received 14.05.22

Е. Соаве, В. Корре, К. Равенсберген,
Дж.Х. Хан, М. Креер, Е. Кирилов, Р. Грімм

РЕЗОНАНСИ ФЕШБАХА
У СЛАБКОМУ ПОЛІ ТА ТРИЧАСТИНКОВІ ВТРАТИ
У ФЕРМІОННОМУ КВАНТОВОМУ ГАЗІ ІЗ ^{161}Dy

За допомогою спектроскопії Фешбаха з високою роздільною здатністю досліджено вироджений поляризований за спіном фермі-газ із атомів ^{161}Dy та виміряно втрати на тричастинкову рекомбінацію в слабких магнітних полях. Для поля біля 1 Гс знайдено 44 резонансні особливості. Також спостерігаються плато з дуже низькими втратами. Для чотирьох типових резонансів вивчено залежність коефіцієнта швидкості тричастинкової рекомбінації від розладування резонанса зміною магнітного поля і від температури. Спостерігалося значне зменшення втрат зі зменшенням температури вже при малих відхиленнях від резонансу. Опис складної поведінки тричастинкових втрат в ферміонному ^{161}Dy є важливим для його подальшого використання в дослідженнях атомних квантових газів.

Ключові слова: ультрахолодні фермі-гази, резонанси Фешбаха, тричастинкова рекомбінація.